HAL
open science

Combustion regimes of hydrogen-air-steam mixtures

Gustav Nyrenstedt, Romain Grosseuvres, Andrea Comandini, Alexandre Bleyer, Ahmed Bentaïb, Nabiha Chaumeix

To cite this version:

Gustav Nyrenstedt, Romain Grosseuvres, Andrea Comandini, Alexandre Bleyer, Ahmed Bentaïb, et al.. Combustion regimes of hydrogen-air-steam mixtures. International Conference on Hydrogen Safety, Sep 2021, Virtual conference, United Kingdom. irsn-04359705

HAL Id: irsn-04359705

https://irsn.hal.science/irsn-04359705

Submitted on 21 Dec 2023

HAL is a multi-disciplinary open access archive for the deposit and dissemination of scientific research documents, whether they are published or not. The documents may come from teaching and research institutions in France or abroad, or from public or private research centers.

L'archive ouverte pluridisciplinaire **HAL**, est destinée au dépôt et à la diffusion de documents scientifiques de niveau recherche, publiés ou non, émanant des établissements d'enseignement et de recherche français ou étrangers, des laboratoires publics ou privés.

Copyright

COMBUSTION REGIMES OF HYDROGEN-AIR-STEAM MIXTURES

Gustav Nyrenstedt[1], Romain Grosseuvres[1], Andrea Comandini[1], Alexandre Bleyer[2], Ahmed Bentaib[2], Nabiha Chaumeix[1]

[1] Institut de Combustion, Aérothermique, Réactivité et Environnement, UPR3021 du CNRS-INSIS, 1C, avenue de la recherche scientifique, 45071 Orléans Cedex 2, France

[2] IRSN, 3, avenue de la Division Leclerc - 92260 FONTENAY AUX ROSES

chaumeix@cnrs-orleans.fr

ABSTRACT

In the case of a severe nuclear power plant accident, hydrogen gas formation may occur, from the core degradation, and cooling water evaporation and subsequent oxidation of zircaloy. These phenomena increase the risk of hazardous combustion events in the reactor, especially when combined with an ignition source. If not handled carefully, these types of accidents can cause severe damage to the reactor building with potential radioactive effects on the environment. Although hydrogen-air combustion has been investigated before, hydrogen-air-steam mixtures remain unstudied under reactor-like conditions. Thus, this study investigated such mixtures' combustion regimes. A closed tube of 318 liters (7.65m tall and 0.23m inner diameter) measures the flame speed, flame propagation and shock wave behaviors for 11-15 %vol hydrogen mixtures combined with 0, 20 or 30 %vol steam, and air. Thus, both the effect of steam and hydrogen content was investigated and compared. The experimental setup combined photomultiplier tubes, pressure sensors, and shock detectors to give a full view of the different combustion regimes. A number of obstacles changed the in-chamber turbulence, during flame propagation, to provide further reactor-like environments. This changed turbulence affected the combustion regimes and enhanced the flame speed for some cases. The results showed varying combustion behaviors depending on the water vapor concentration, where a higher concentration meant a lower flame speed, reduced pressure load, and sometimes combustion extinction. At 0 %vol steam dilution, the flame speed remained supersonic for all H_2 concentrations, while at 30 %vol steam dilution, the flame speed remained subsonic for all H_2 concentrations. Thus, with high levels of steam dilution, the risk for shock waves, leading to potential reactor building destruction, decreases.

1.0 INTRODUCTION

Nuclear reactor electricity generation presents one of the cleanest alternatives when it comes to life-cycle CO_2 emissions [1-3]. However, the safety concerns for potential accidents remain, especially after the Fukushima accident [4]. This accident involved hydrogen (H_2) explosions, causing structural damage, leading to the release of radioactive material to the surroundings [5].

Light water nuclear reactors can in general form H_2 through for example reactions between the zircaloy fuel-coating and the surrounding steam [6, 7]. This H_2-generation occurs during reactor overheating since the steam generation and reaction initiation require certain temperature levels. To avoid this overheating, occurring during cooling system failure, several nuclear power plants (NPP) utilize pressure release valves allowing H_2 -and steam flow to the reactor containment building.

To avoid NPP H_2-ignition, with risk for detonation [8, 9], a thorough understanding of combustion behavior at NPP-like conditions is needed. Fundamental studies [10-12] concluded a H_2 lean flammability limit at 4 %vol when mixed with air at atmospheric pressure and temperature. However, the laminar flame speed remains low at low equivalence ratios (ER) [11, 13] suggesting a low detonation probability. For the NPP, the transition limit from non-hazardous to hazardous conditions must be known.

To understand this transition limit, different CFD-simulations [14, 15] predict the combustion regimes and flame propagation inside the NPP containment building. The mere building size represents a

computational challenge leading to large mesh sizes [16]. Thus, the mesh sizes needed for accurately predicting detonation waves cannot be reached. Instead, different assumptions are made which need to be validated against experimental data.

Previous studies aimed to provide this validation data [17] for varying H_2 concentrations and temperatures. These studies included turbulence created from different obstacle configurations to further mimic the NPP environment. A specific vertical combustion vessel, aiming to mimic the NPP, performed the experiments showing little or no risk for detonation at H_2 concentrations below 11 %vol. However, this behavior changes with diluent addition [18].

The present study investigates (in the framework of the MITHYGENE project) how steam, potentially released together with the H_2 in a NPP accident, affects the combustion regimes with respect to diluting the mixtures. A vertical, bottom-ignited vessel [17] evaluated H_2-concentrations, ranging from 10 to 15 %vol, mixed with air and steam (0, 20 or 30 %vol). This work provides new insights on how steam improves or deteriorates the detonation risk during a nuclear reactor accident.

2.0 METHODOLOGY

This section summarizes and describes the different experimental and post-processing methods used for this article.

2.1 Experimental Setup

A 7.65m tall vertical combustion chamber (ENACCEF2) [17, 19] performed the H_2/air/steam experiments. ENACCEF2 consists of nine different sections forming a cylindrical tube (230 mm internal diameter), where each section includes three photomultiplier tubes (PMs) placed with a 150 mm height difference. These PMs detect light around a 306 nm wavelength via a 5 mm diameter optical passage through the ENACEFF2 wall. The small optical passage diameter allows flame detection via a thin horizontal sheet (using a plano-convex lens of 100 mm focal length and a slit of 1 mm thickness). Each section also contains a pressure sensor. The two lowest sections, usually experiencing subsonic combustion, wield PCB 113B03 sensors suitable for that regime. The other sections use Kistler 601CA sensors to better account for the possible supersonic combustion here. The top section also includes a Kistler sensor at the end wall. A silicon coating protects all pressure sensors from hot gases ensuring measurement accuracy. To further follow the shock waves, the top sections used five shock detectors.

In ENACCEF2, ignition occurs at the bottom flange, by a spark plug, inducing an upwards flame propagation. This study also included nine annular obstacles at the bottom sections (from a height of 0.638m up to 2.478m). All obstacles used a blockage ratio of 0.63, defined as follows:

$$BR = 1 - (d/D)^2 \quad (1)$$

Where d is the inner obstacle diameter [m] and D the ENACCEF2 interior tube diameter [m]. The obstacles aim to mimic the possible turbulence created from real obstacles in a nuclear reactor containment building. To further mimic real conditions, an electrical resistance heating system accompanies each section. Several temperature sensors regulate this heating system to ensure a close to constant temperature along the tube. H_2 is a light species and the constant temperature ensures minimum in-vessel mixture stratification.

All experiments used H_2-fuel with air as oxidizer, while steam diluted some experiments. The gas injection system included species-specific Bronkhorst, F-201CV mass flowmeters to ensure a correct species concentration. The water is first supplied to a heated mixing tank where the liquid transforms to steam. After the mixing tank, three injection lines (at different heights) supplied the ENACCEF2 with the final gas mix. This approach minimized concentration gradients. Furthermore, a micro-GC (SRA Instruments) analysis verified the mixture compositions and homogeneity by sampling the gas composition at different heights.

2.2 Experimental Procedures and Conditions

All experiments followed a number of steps as: chamber filling up to 1 bar by supplying the gases as described above; gas sampling at four different heights coupled with micro-GC analyses to exclude concentration gradients and verify the mixture composition; spark plug triggering with following combustion initiation; binary data collection via a Hioki MR8827 and a Hioki MR8847-03; and data conversion (from binary to text format) with following post-processing. This data collection -and conversion approach allowed large file sizes and small time-steps at a roughly ten times faster rate compared to previous studies. Every experimental condition was repeated at least three times to ensure consistency.

This article focuses on the effect of steam dilution for H_2/air mixtures at NPP-relevant conditions. Tab. 1 summarizes these conditions where three H_2 concentrations (ER = 0.294, 0.356 and 0.42) and three steam concentrations (0, 20 and 30 %) alternated to create a total of nine experimental conditions. All cases utilized an initial temperature of 140 °C, and an initial pressure of 1 bar inside the ENACCEF2 tube. The initial temperature aimed to mimic NPP conditions during an accident and ensured that the water be present as vapor.

Table 1. Experimental conditions

Case	Steam Conc. [%vol]	H_2 in the dry mixture[%vol]	ER
1-3	0 %	11%, 13%, 15%	0.294, 0.356, 0.42
4-6	20 %		
7-9	30 %		

2.3 Data Analysis and Calculations

Several analyses -and calculation steps followed after the binary data conversion. A pre-flame detection PM signal analysis set the initial signal level at zero. Fig. 1 shows a typical PM voltage signal from flame detection, and highlights the maximum slope of the first peak. This slope calculates the flame speed by indicating the flame detection time. This article defines the flame detection time as the time when the maximum slope line cuts the horizontal zero-axis (around 0.6 s from spark initiation in Fig.1). Such a definition ensures that the flame detection time reflects the actual flame passing and avoids light-pollution from a nearby flame (that did not yet reach the PM) [20]. The velocity calculations then follow from knowing both the flame detection time and the PM placement height as follows:

$$\boldsymbol{v_i} = \frac{(\boldsymbol{h})_{i+1}-(\boldsymbol{h})_{i-1}}{(\boldsymbol{t})_{i+1}-(\boldsymbol{t})_{i-1}} \tag{2}$$

Where v denotes the flame speed [m/s], *i* the PM number, h the PM placement height [m from the spark plug], and t the flame detection time [seconds from spark initiation].

The pressure sensor signals rendered knowledge both on pressure rise (from combustion) and shock wave behavior. All pressure signals were converted to bar via earlier performed calibrations at relevant conditions. Fig.2 shows the pressure traces for an example case, from five out of ten sensors. The leading shock (red dashed line) gives a rapid pressure rise when passing a sensor and can thus be easily detected. The shock wave then reflects at the ENACCEF2 top flange and travels back downwards. This reflected shock (blue dashed line in Fig.2) follows the leading shock behavior with a following pressure jump. The shock wave time calculation differs from the PM signal flame detection.

Instead of the maximum slope method, the shock wave time follows from pinpointing the start of rapid pressure rise. The shock wave speed follows from the shock wave trajectory, using a polynomial fit.

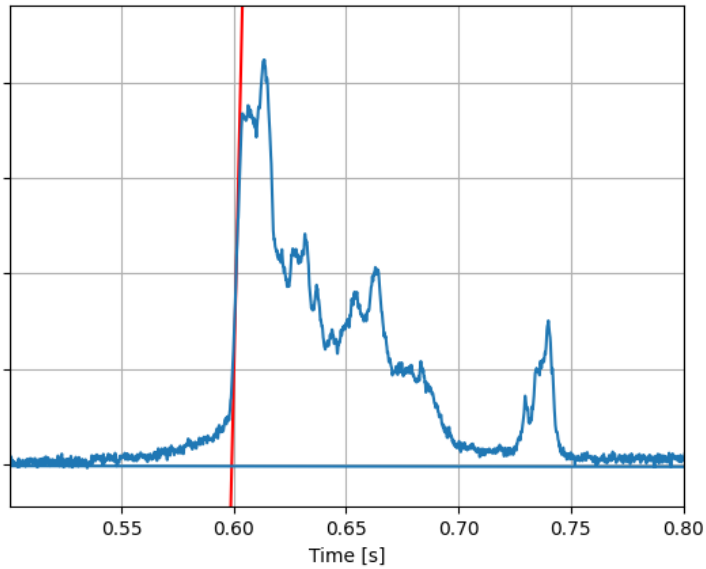

Figure 1. Example PM signal, as a function of time from spark initiation, illustrating the maximum slope (red line) used for flame speed calculations

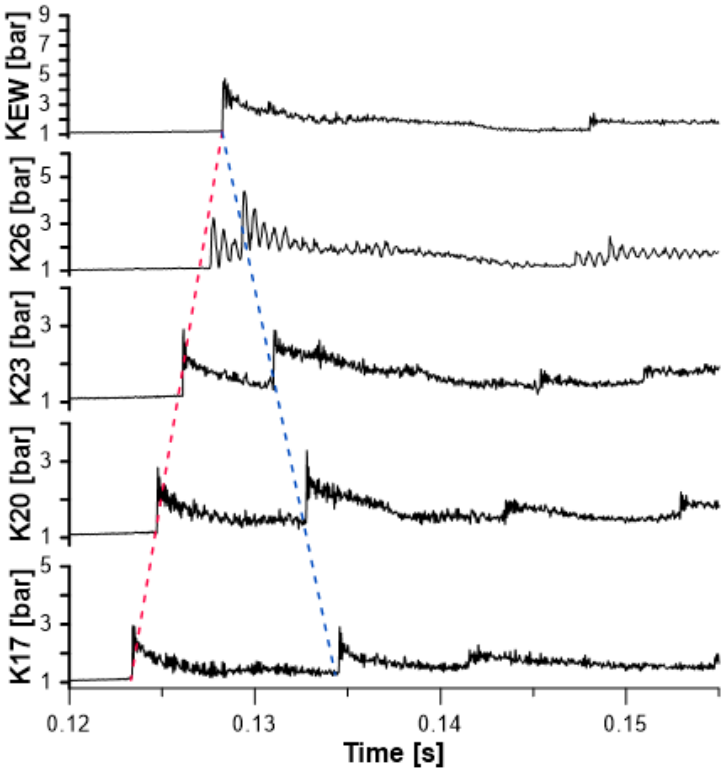

Figure 2. Pressure sensor data [bar] for an example case to illustrate the leading shock (red dashed line) and reflected shock (blue dashed line). This shock wave detection later calculates the shock speed. K indicates the pressure sensor type (Kistler) while the numbers 17, 20, 23 etc. indicate an ascending sensor placement height. KEW denotes the end-wall Kistler sensor.

2.4 Fundamental Flame Parameters and Simulations

To classify the experimental results, this study investigates several flame parameters. Dorofeev et al. [21] indicated a relationship for determining the experimental geometry scale dependence. Eq. 3 highlights the ratio between the integral length scale of turbulence (L_T) and the flame thickness (δ). When this ratio exceeds 100, the experiment is considered independent of the geometry scale. Here, L_T is equivalent to the inner diameter of the ENACCEF2 facility, which equals 230 mm. The Zeldovich number (β) correlates to a mixture's reactivity. Eq. 4 shows one way to calculate β, from the activation energy (E_a), the universal gas constant (R), the flame temperature (T_b), and the initial temperature (T_u). The E_a follows from the correlation described in Eq. 5, where S_L denotes the laminar flame speed.

$$\frac{L_T}{\delta} > 100 \quad (3)$$

$$\beta = \frac{E_a}{R{T_b}^2}(T_b - T_u) \quad (4)$$

$$2 * \ln(S_L) \propto \frac{E_a}{RT_b} \quad (5)$$

The expansion ratio (σ) follows from Eq. 6, where ρ_u and ρ_b denote the unburnt and burnt gas densities. Dorofeev et al. [21] also showed how a critical expansion ratio [σ^*] can be used to determine the fast flame regimes. Ciccarelli et al. [22] later established a polynomial fit to known experimental compositions (see Eq. 7). If the σ-value remains above σ^*, the flame is considered fast. Eq. 8 reveals another fast-flame definition. A ratio, between the maximum flame speed [v_{max}] and the speed of sound in the burnt gases (c_{BG}), above 0.5 indicates a fast flame [21].

$$\sigma = \frac{\rho_u}{\rho_b} \quad (6)$$

$$\sigma^* = -0.00285\beta^2 + 0.3823\beta - 2.2078 \quad (7)$$

$$\frac{v_{max}}{c_{BG}} > 0.5 \quad (8)$$

Equilibrium and flame simulations in COSILAB [23] calculated the flame parameters used here. The Mével mechanism [24] was used for all conditions to ensure consistency. For these simulations, the laminar flame speed indicated no flame propagation with 20 -or 30 % steam-addition. Thus, an exponential fit (based on the data points without steam) estimated the laminar flame speed for the steam-conditions here. The β-determination followed a procedure where the unmeasured data points were decided via a polynomial fit. In general, all flame parameter calculations followed a previous study [25]

3.0 RESULTS

This section evaluates and describes the different phenomena experienced and includes an analysis for case-to-case difference, flame speed calculations and shock wave analyses.

3.1 Data Reproducibility

Every experimental condition includes at least three separate runs to ensure accuracy. Fig. 3 compares the three runs at 20 %vol steam and ER0.356 to highlight the run-to-run differences. The detection height indicates the spark plug-to-flame distance as detected by the PMs. Fig.3a shows clear trends, confirmed by the different runs, although small local differences exist. The first speed-peak (just before 3m) and the second speed-peak (around 4.5m) occur for all three runs while the amplitude differs slightly at high flame speeds. Due to the fast flame, Fig.3b shows only minor time differences between the three runs. This behaviour suggests good experimental accuracy, especially for high flame speeds.

Some experimental conditions suffer from larger case-to-case differences. Fig.4 highlights the 30 %vol steam and ER0.356 case where the flame quenches for all runs inside the obstacle-region. However, re-ignition occurs only for two of three runs (see Fig.4). These two runs (362 and 364) experience the re-ignition after the obstacle-region where the flame travels in several directions. Fig.4a indicates a negative flame speed following from the flame traveling downwards. However, Fig.4a also indicates an upwards traveling flame (positive speed) meaning a three-dimensional re-ignited flame propagation. The later data averaging procedure ignores the outlier runs (with largely differing results).

When occurring, GC analyses (by post-experimental gas sampling) confirmed the flame extinction by confirming no H_2 consumption above the extinction height. This procedure ensured that extinction actually occurred and ruled out non-detected re-ignitions, occurring after the signal collection end time.

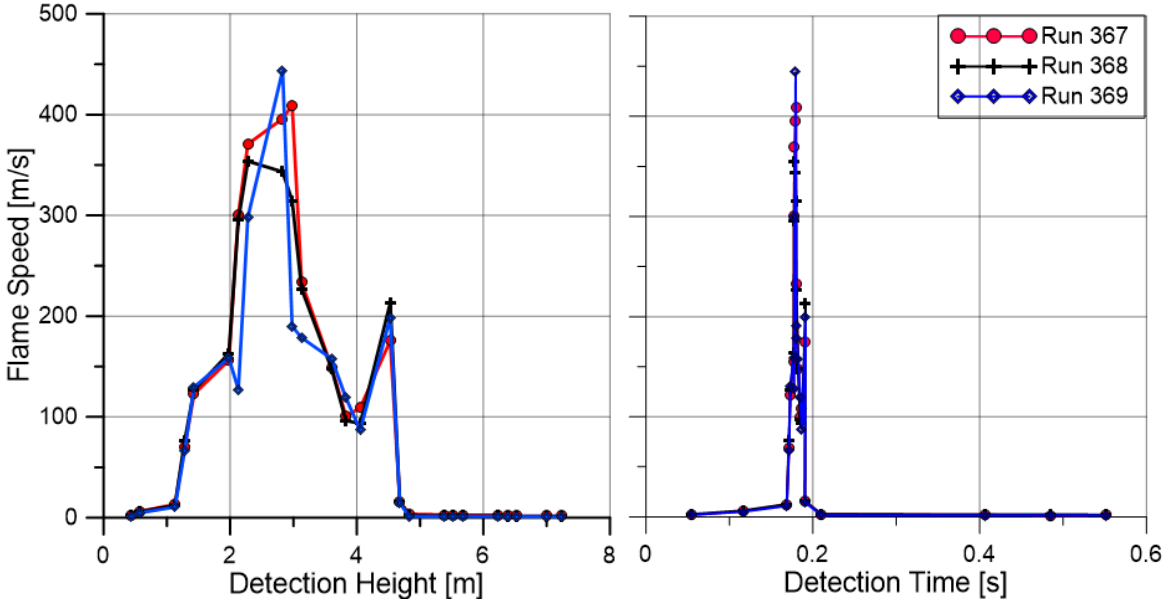

Figure 3. Flame speed [m/s], vs PM flame detection height (a) and PM flame detection time (b), comparisons between different experimental runs for 20 %vol steam at ER0.356

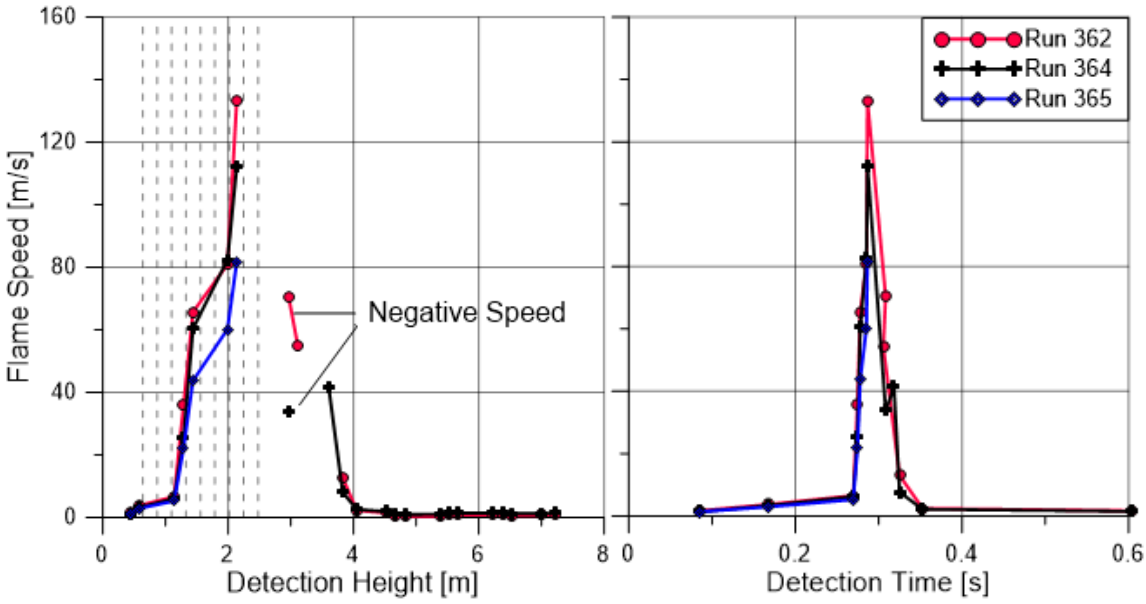

Figure 4. Flame speed [m/s], vs PM flame detection height (a) and PM flame detection time (b), comparisons between different experimental runs for 30 %vol steam at ER0.356. The vertical dashed lines indicate obstacle heights.

3.2 H_2/Air/Steam Combustion Regimes

This section describes the effects of ER and steam dilution on H_2/air mixtures. The results presented were obtained by averaging over experiments conducted at similar initial conditions. For any given ER, an increased steam dilution decreases the flame speed (see Fig.5a). At the low ER = 0.294, this phenomenon becomes even more apparent. Fig.5a depicts how the maximum flame speed falls by around 400 m/s when moving from 0 to 20 %vol steam dilution. When increasing the steam dilution further, to 30 %vol, the maximum flame speed again falls slightly and occurs later.

The higher ER cases (0.356 and 0.42) require more steam dilution to obtain the low flame speed encountered for the ER=0.294 case. Fig.5a shows how the maximum flame speed remains high at 20 %vol steam dilution, for the ER=0.356 and ER=0.42 cases. The maximum flame speed, around 400 m/s, remains close to supersonic conditions (speed of sound = 448 m/s in the fresh gases at ER=0.42 and 20 %vol steam dilution) with the following risk of shock wave creation. This risk disappears at 30 %vol steam dilution, independent of ER. Fig.5b concludes that the maximum flame speed remains below 200 m/s for all H_2 concentrations. In the NPP, a 30 %vol steam dilution thus corresponds to a lower risk of containment building damage.

The H_2 concentration matters only to a small extent at 0 or 30 %vol steam dilution. Fig.5b shows how the flame speed remains high, independent of H_2 concentration, at 0 %vol steam dilution. Simultaneously, the flame speed remains low for 30 %vol steam dilution. However, the H_2 concentration changes the flame speed drastically at 20 %vol steam dilution. As described above, the maximum flame speeds remain close to the supersonic region for the ER0.356 and ER0.42 cases. Thus, in the case of an NPP accident, the experienced H_2 concentration becomes increasingly important if a 20 %vol steam dilution is present.

As discussed above, shock waves can occur at flame speeds above the speed of sound. This study found a borderline between the ER=0.356 and ER=0.42 cases at 20 %vol steam dilution. Fig.6a indicates no shock wave behaviors at ER=0.356 while a clear shock wave follows from the ER=0.42 case (see Fig.6b). This borderline corresponds to the earlier observed flame speeds, where the ER=0.356 maximum flame speed falls below 400 m/s for a 20 %vol steam dilution.

Fig.6b further shows how the shock wave intensity (in terms of maximum pressure) reduces as it passes the obstacle region (for PCB2 and PCB5). This is probably caused by the turbulence created here. In general, the leading shock wave speed (see Fig.7) decreased as a function of time due to fluid mechanical effects, such as friction. Fig.7 further correlates how an increased ER elevates the leading shock wave speed. An ER increase from 0.294 to 0.42 gives a roughly 100 m/s higher shock wave speed here.

The steam addition affects the shock wave speed only to a small extent (see Fig.7). The initial shock wave speed decreases slightly while the speed reduction during propagation becomes smaller. Thus, the top of ENACCEF2 experiences a higher shock wave speed for 20 %vol steam dilution compared to 0 %vol (at ER=0.42). However, the speed of sound increases with steam dilution which affects the Mach number. In the NPP, the shock wave speed influences the severity of a potential ignition. Here, if the shock wave occurs, the steam addition seams to have only a small effect.

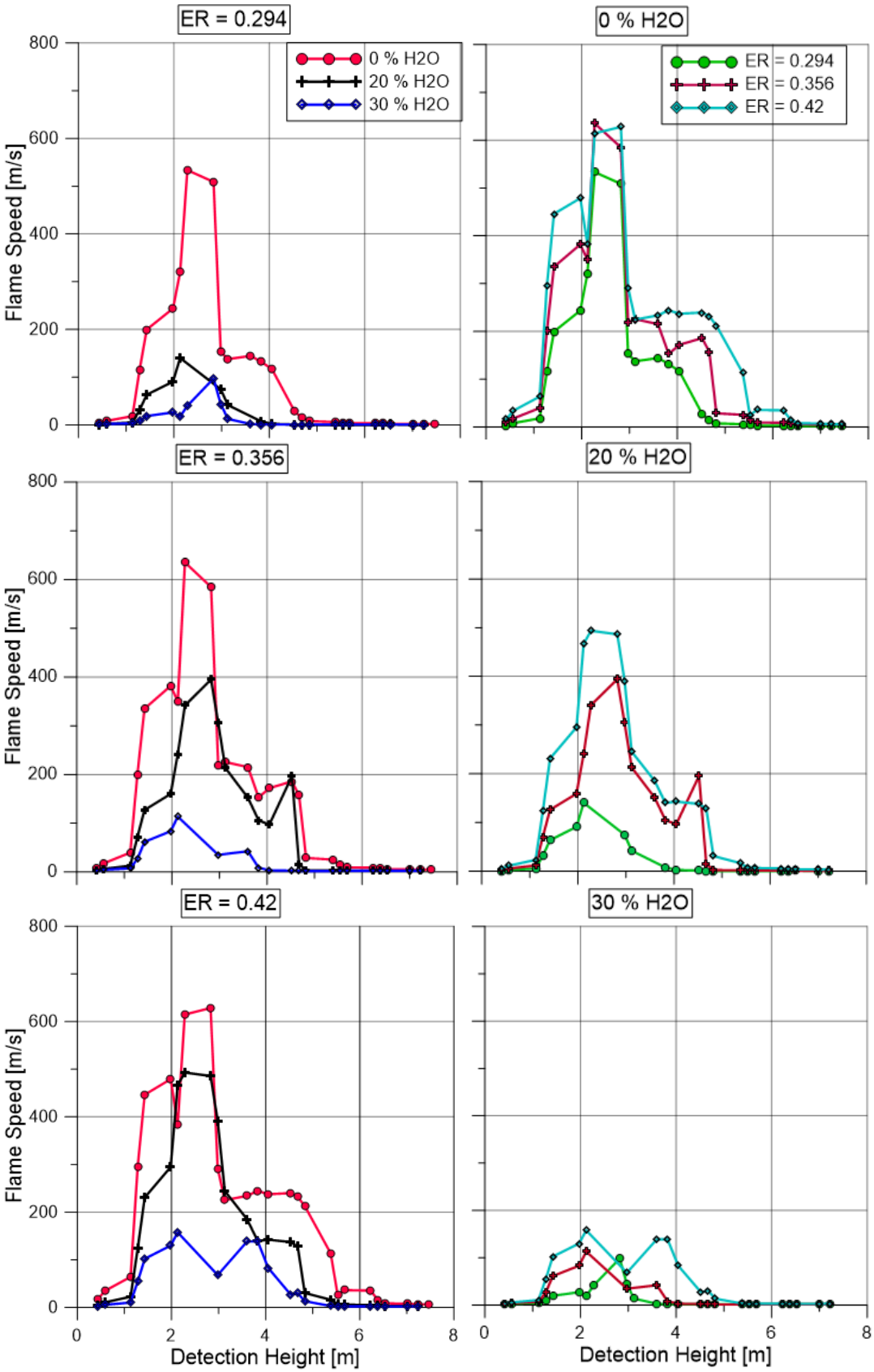

Figure 5. Flame speed [m/s] as a function of PM flame detection distance, from the spark plug, for all cases. The left-hand side graphs (a) compare different H_2O concentrations at every ER, while the right-hand side graphs (b) compare different H_2 concentrations.

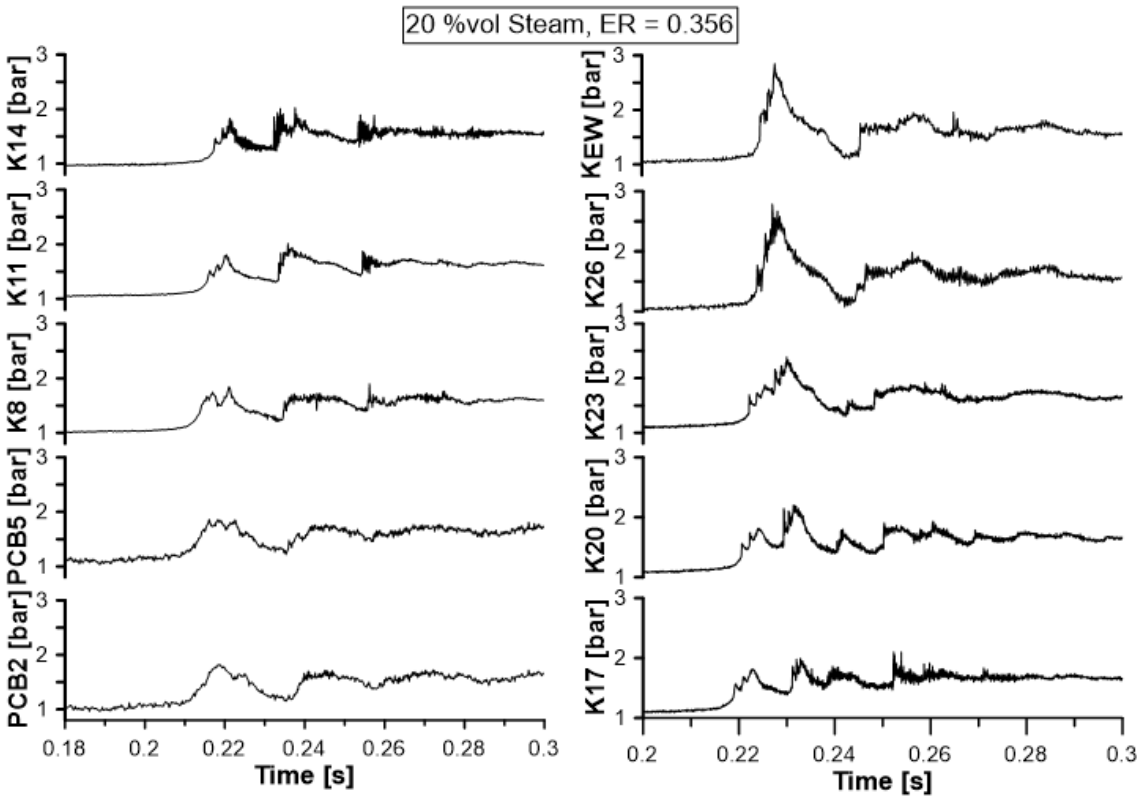

(a)

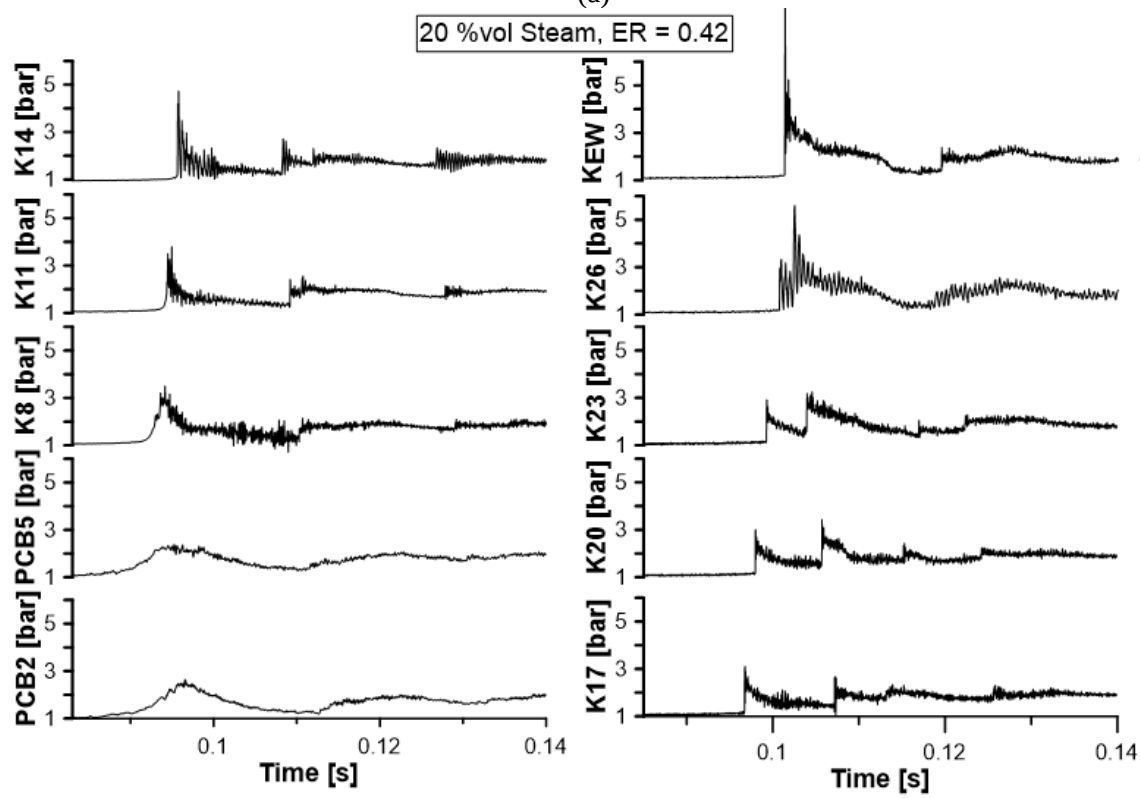

(b)

Figure 6. Pressure sensor detection at different heights for the cases utilizing 20 %vol steam dilution at ER0.356 (a) and ER0.42 (b). PCB and K denote the pressure sensor type (PCB or Kistler) while 2, 5, 8 etc. denote the sensor placement position

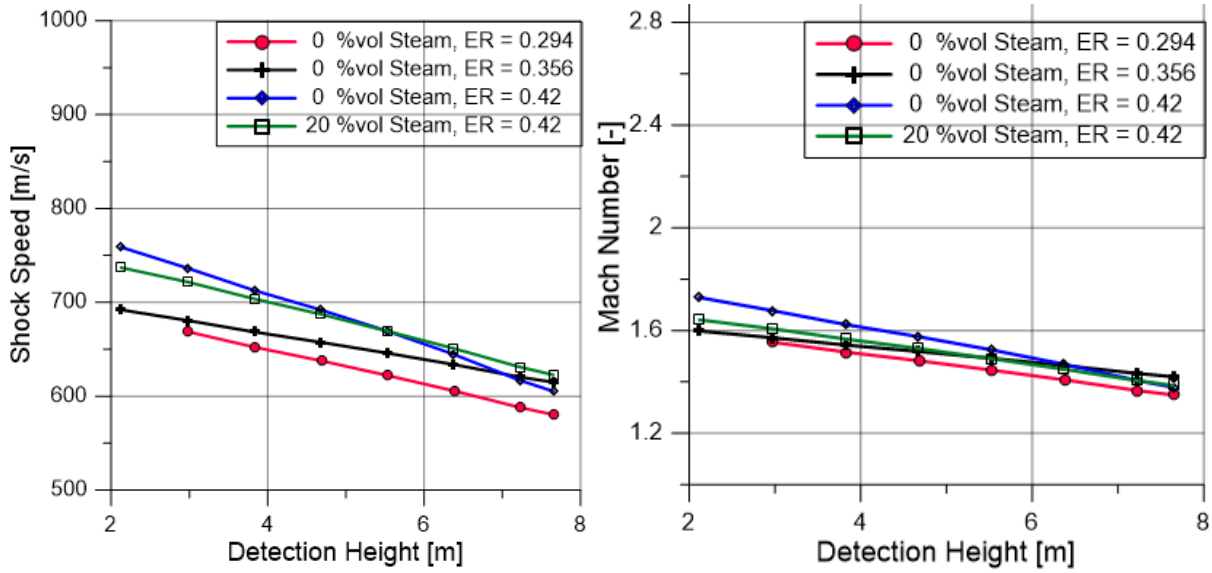

Figure 7. Leading shock wave speed [m/s] and Mach number [-] for all cases with shock waves

3.3 Fundamental Flame Parameters

This section describes and determines fast flame regimes for the evaluated conditions. The ratio between L_T and δ falls well above 1000 for all experimental cases here. Thus, the evaluated conditions remain independent of scale, according to Eq. 2. Figure 8 sorts out fast flame conditions from slow flame conditions by utilizing Eq. 6, as described earlier. All data points containing 30 % steam experience slow-flame behaviour. The ER=0.294 case with 20 % steam also falls among the slow flames. All other conditions sustain fast flames according to the criterion used here. From now on, red dots indicate fast flames while black dots indicate slow flames, in the graphs.

Figure 9 compares the fast-flame criterion discussed above with the fast-flame criterion (labelled the sigma-criterion) described by Cicarelli et al. [22]. All the fast flames are also considered fast with respect to the sigma-criterion. However, two of the slow flame conditions (the one at ER=0.294 with 20 % steam, and the one at ER=0.42 with 30 % steam) fall just above the critical expansion ratio, indicating that these conditions render fast flames. Thus, the two fast-flame criteria do not fully agree under the present experimental conditions.

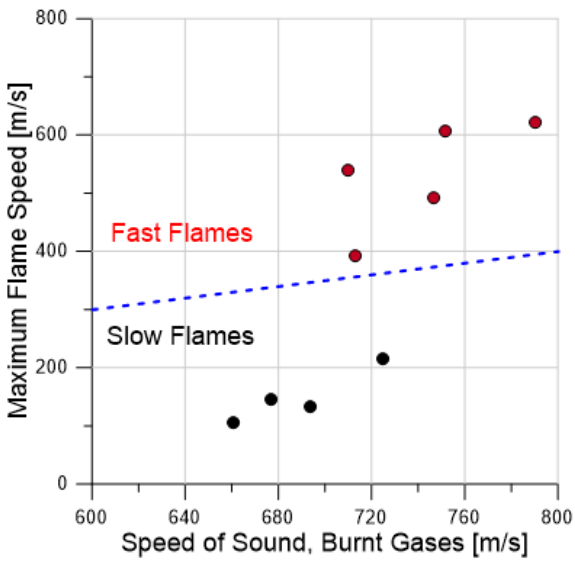

Figure 8. The maximum measured flame speed [m/s] as a function of the speed of sound in the burnt gases [m/s]. The dashed line denotes the fast-flame criterion as $v_{max} > 0.5*c_{BG}$

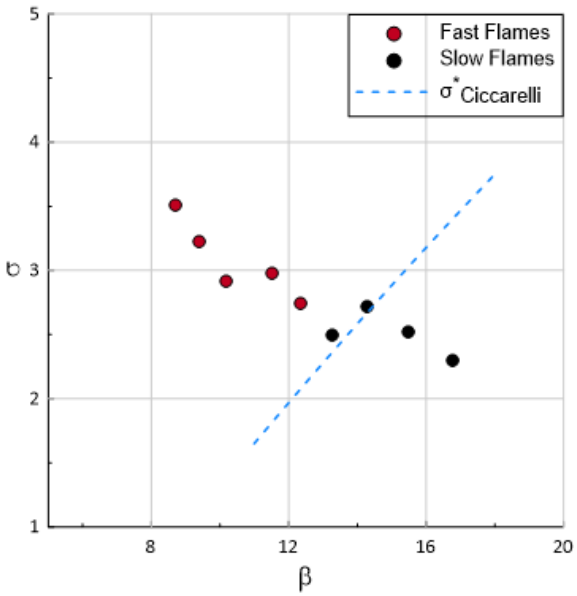

Figure 9. Expansion ratio as a function of the Zeldovich number plotted together with the critical expansion ratio (blue dashed line) as decided by Cicarelli et al. [22]

A third fast-flame criterion will be considered here. Dorofeev et al. [21] provided a sigma-criterion similar to the one later established by Cicarelli et al. Figure 10 compares the fast -and slow flames, as established by Eq. 6, with Dorofeev's criterion. Here, only three experimental points experience fast flames according to the Dorofeev-criterion. This opposes the five fast flame conditions by Eq. 6, and the seven fast flame conditions by the Cicarelli-criterion. In addition, one of the data points lies on the limit-line in Figure 10, indicating difficulties to determine if it is a fast flame or not with the Dorofeev-criterion. This section concludes that neither the Cicarelli -nor the Dorofeev criteria suit these experimental conditions for determining fast-flame regimes. Thus, more experiments with H_2/air/steam mixtures are needed to establish relevant sigma-criteria.

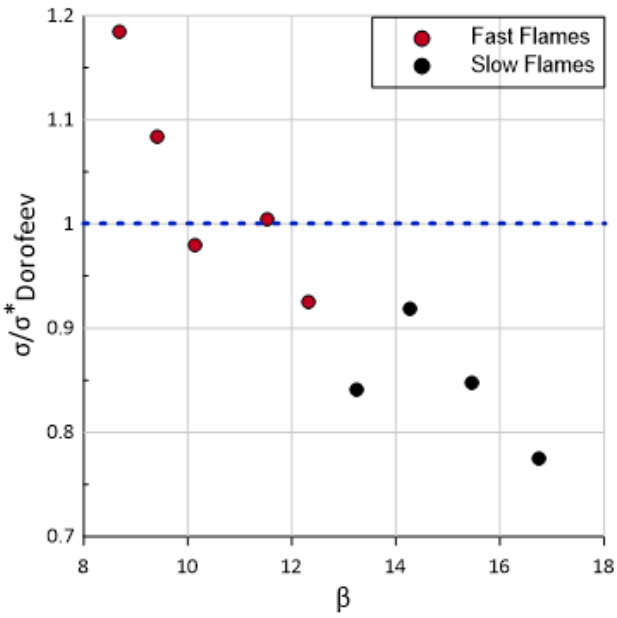

Figure 10. The present study's expansion ratios normalized by the critical expansion ratios as decided by the polynomial fits from Dorofeev et al. [21], plotted against the Zeldovich number. The blue dashed line indicates the fast flame limit as decided by Dorofeev's sigma-criterion

4.0 CONCLUSIONS

This study investigated combustion behaviors in a vertical vessel, designed to mimic nuclear power plant conditions. This facility enabled detailed flame acceleration studies of fuel/air/diluent mixtures in a confined environment, with a variety of diagnostics to characterize the flame propagation history and the subsequent pressure loads. The detailed data output from this study validate future CFD codes for nuclear safety applications. In this work, H2/air mixtures diluted with steam were investigated in terms of flame speed and shock waves to evaluate the potential effects of a combustion event in a nuclear power plant. Equivalence ratios of 0.294, 0.356 and 0.42 investigated the steam addition effects at 0, 20 -and 30 %vol. The main conclusions follow as:

- Steam dilution affects the combustion behavior largely where a 30 %vol steam dilution completely prevents the creation of shock waves at the tested equivalence ratios.
- The H2 concentration gives little or no effect on the combustion behavior at 0 or 30 %vol steam dilution. At 0 %vol, the flame speed remains supersonic while at 30 %vol, the flame speed remains subsonic.
- Steam dilution prevents shock wave creation to a large extent due to the reduced flame speed.
- If shock waves occur, the steam dilution has little or no effect on the leading shock wave speed.
- Further experiments are needed to establish expansion ratio correlations for fast-flame characterization

ACKNOWLEDGEMENTS

The authors acknowledge the financial support of the French government within the program "Investissement d'Avenir - MITHYGENE grant agreement n°ANR 11-RSNR-0015"

ABBREVIATIONS

ER – equivalence ratio

EW – end wall

GC – gas chromatograph

H_2 - hydrogen

K – Kistler

NPP - nuclear power plant

PM – photomultiplier tube

REFERENCES

1. van der Zwaan, B., 2013. The role of nuclear power in mitigating emissions from electricity generation. *Energy Strategy Reviews*, *1*(4), pp.296-301.
2. Kharecha, P.A. and Hansen, J.E., 2013. Prevented mortality and greenhouse gas emissions from historical and projected nuclear power. *Environmental science & technology*, *47*(9), pp.4889-4895.
3. Siddiqui, O. and Dincer, I., 2017. Comparative assessment of the environmental impacts of nuclear, wind and hydro-electric power plants in Ontario: a life cycle assessment. *Journal of Cleaner Production*, *164*, pp.848-860.
4. Visschers, V.H. and Siegrist, M., 2013. How a nuclear power plant accident influences acceptance of nuclear power: Results of a longitudinal study before and after the Fukushima disaster. *Risk Analysis: An International Journal*, *33*(2), pp.333-347.
5. Nuclear Energy Agency, 2021, *Fukushima Daiichi Nuclear Power Plant Accident, Ten Years On, NEA No. 7558*
6. Suman, S., Khan, M.K., Pathak, M., Singh, R.N. and Chakravartty, J.K., 2015. Hydrogen in Zircaloy: Mechanism and its impacts. *international journal of hydrogen energy*, *40*(17), pp.5976-5994.
7. Courty, O., Motta, A.T. and Hales, J.D., 2014. Modeling and simulation of hydrogen behavior in Zircaloy-4 fuel cladding. *Journal of Nuclear Materials*, *452*(1-3), pp.311-320.
8. Yanez, J., Kuznetsov, M. and Souto-Iglesias, A., 2015. An analysis of the hydrogen explosion in the Fukushima-Daiichi accident. *International Journal of Hydrogen Energy*, *40*(25), pp.8261-8280.
9. Nishimura, T., Hoshi, H. and Hotta, A., 2015. Current research and development activities on fission products and hydrogen risk after the accident at Fukushima Daiichi nuclear power station. *Nuclear Engineering and Technology*, *47*(1), pp.1-10.
10. Liu, X. and Zhang, Q., 2014. Influence of initial pressure and temperature on flammability limits of hydrogen–air. *International Journal of Hydrogen Energy*, *39*(12), pp.6774-6782.
11. Grosseuvres, R., Comandini, A., Bentaib, A. and Chaumeix, N., 2019. Combustion properties of H2/N2/O2/steam mixtures. *Proceedings of the Combustion Institute*, *37*(2), pp.1537-1546.
12. Kuznetsov, M., Kobelt, S., Grune, J. and Jordan, T., 2012. Flammability limits and laminar flame speed of hydrogen–air mixtures at sub-atmospheric pressures. *International journal of hydrogen energy*, *37*(22), pp.17580-17588.
13. Ciccarelli, G., Chaumeix, N., Mendiburu, A.Z., N'Guessan, K. and Comandini, A., 2019. Fast-flame limit for hydrogen/methane-air mixtures. *Proceedings of the Combustion Institute*, *37*(3), pp.3661-3668.
14. Bentaib, A., Meynet, N. and Bleyer, A., 2015. Overview on hydrogen risk research and development activities: methodology and open issues. *Nuclear Engineering and Technology*, *47*(1), pp.26-32.
15. Nicolás-Pérez, F., Velasco, F.J.S., García-Cascales, J.R., Otón-Martínez, R.A., Bentaib, A. and Chaumeix, N., 2020. Evaluation of different models for turbulent combustion of hydrogen-air mixtures. Large Eddy Simulation of a LOVA sequence with hydrogen deflagration in ITER Vacuum Vessel. *Fusion Engineering and Design*, *161*, p.111901.
16. Bocanegra, R., Di Marcello, V., Sánchez-Espinoza, V.H. and Jiménez, G., 2018. Fukushima Unit 2 Accident Simulation With MELCOR 2.1. *Journal of Nuclear Engineering and Radiation Science*, *4*(2).
17. Grosseuvres, R., Bentaïb, A. and Chaumeix, N., 2019, July. Effect of initial temperature and temperature gradient on H2/Air flame propagation in confined area. In *27 International Colloquium on the Dynamics of Explosions and Reactive Systems*.
18. Sathiah, P., Komen, E. and Roekaerts, D., 2015. The role of CFD combustion modeling in hydrogen safety management–III: Validation based on homogeneous hydrogen–air–diluent experiments. *Nuclear Engineering and Design*, *289*, pp.296-310.
19. Bentaïb, A., Chaumeix, N., Grosseuvres, R., Alexandre, B., Gastaldo, L., Ludovic, M., Jallais, S., Vyazmina, E., Kudriakov, S., Studer, E. and Dehbi, A., 2018, October. ETSON-MITHYGENE

benchmark on simulations of upward flame propagation experiment in the ENACCEF2 experimental facility. In *12th International Topical Meeting on Reactor Thermal-Hydraulics, Operation, and Safety (NUTHOS-12)*.

20. O. Mathieu, J. Goulier, F. Gourmel, M.S. Mannan, N. Chaumeix, E.L. Petersen, (2015). Experimental study of the effect of CF3I addition on the ignition delay time and laminar flame speed of methane, ethylene, and propane, Proc. Combust. Inst, 35(3), 2731-2739, http://dx.doi.org/10.1016/j.proci.2014.05.096
21. Dorofeev, S.B., Kuznetsov, M.S., Alekseev, V.I., Efimenko, A.A. and Breitung, W., 2001. Evaluation of limits for effective flame acceleration in hydrogen mixtures. *Journal of loss prevention in the process industries*, *14*(6), pp.583-589.
22. Ciccarelli, G., Chaumeix, N., Mendiburu, A.Z., N'Guessan, K. and Comandini, A., 2019. Fast-flame limit for hydrogen/methane-air mixtures. *Proceedings of the Combustion Institute*, *37*(3), pp.3661-3668.
23. COSILAB, Rotexo GmbH & Co KG, http://www.rotexo.com.
24. Mével, R., Javoy, S., Lafosse, F., Chaumeix, N., Dupré, G. and Paillard, C.E., 2009. Hydrogen–nitrous oxide delay times: Shock tube experimental study and kinetic modelling. *Proceedings of The Combustion Institute*, *32*(1), pp.359-366.
25. Grosseuvres, R., Comandini, A., Bentaib, A. and Chaumeix, N., 2019. Combustion properties of H2/N2/O2/steam mixtures. *Proceedings of the Combustion Institute*, *37*(2), pp.1537-1546.